Selective Laser Sintering vs. Multijet Fusion as a Basic Comparative Study of PA12 Polyamide Based on Accuracy and Significant Indicators

Andrej Czan [1*], Natalia Czanova [2], Ivan Kuric [3], Tatiana Czanova [4], Jozef Holubjak [5],

Andrej Czan [6], Dominik Krisak [7]

[1]   Department of Machining and Production Engineering, Faculty of Mechanical Engineering - University of Žilina, Univerzitna8215/1, 010 26, Žilina, SLOVAKIA. E-mail: andrej.czan2@fstroj.uniza.sk

[2]   Department of Machining and Production Engineering, Faculty of Mechanical Engineering - University of Žilina, Univerzitna8215/1, 010 26, Žilina, SLOVAKIA. E-mail: natalia.czanova@fstroj.uniza.sk

[3]   Department of Automation and Production Systems, Faculty of Mechanical Engineering - University of Žilina, Univerzitna8215/1, 010 26, Žilina, SLOVAKIA. E-mail: ivan.kuric@fstroj.uniza.sk

[4]   Department of Machining and Production Engineering, Faculty of Mechanical Engineering - University of Žilina, Univerzitna8215/1, 010 26, Žilina, SLOVAKIA. E-mail: tatiana.czanova@fstroj.uniza.sk

[5]   Department of Machining and Production Engineering, Faculty of Mechanical Engineering - University of Žilina, Univerzitna8215/1, 010 26, Žilina, SLOVAKIA. E-mail: jozef.holubjak@fstroj.uniza.sk

[6]   Department of Machining and Production Engineering, Faculty of Mechanical Engineering - University of Žilina, Univerzitna8215/1, 010 26, Žilina, SLOVAKIA. E-mail: andrej.czan@fstroj.uniza.sk.

[7]   Department of Machining and Production Engineering, Faculty of Mechanical Engineering - University of Žilina, Univerzitna8215/1, 010 26, Žilina, SLOVAKIA. E-mail: dominik.krisak@fstroj.uniza.sk

*   Corresponding author andrej.czan2@fstroj.uniza.sk

Abstract: Selective laser sintering (SLS) and Multijet fusion (MJF) are additive technologies that are the most widely used techniques for powder materials for the production of polymer parts, as they offer high flexibility of complex and articulated components, specific properties to metallic materials and serial production. The main requirement of technological equipment is whether they are precise and precise. However, due to the different technological processes, they differ significantly mainly in the source of thermal energy for melting the powder material, as well as the innovative use of processes to promote material consolidation and prevent thermal reflow on the contours of the components. One type of powder made of polyamide (PA 12) was applied to the production of samples using SLS and MJF additive technologies. Experimental analysis of samples ensures the initial identification of hardness, which characterizes the influence of the technology on mechanical properties in the form of hardness. Subsequently, the dimensional and shape accuracy of the produced samples was analyzed, which provides input data to identify the accuracy and precision of the applied technological equipment. Other experimental experiments were focused on the texture and precision of the surface such as straightness, waviness and roughness. In general, the applied SLS and MJF technologies show both advantageous and disadvantageous properties, which need to be monitored for the purpose of appropriate selection to ensure the best accuracy and precision of the manufactured components.

Keywords: Hardness,mechanical properties, selective laser sintering (SLS), multijet fusion (MJF), powder material

Porównanie selektywnego spiekania laserowego (SLS) i technologii MultiJet Fusion (MJF) poliamidu PA12 w oparciu o dokładność i parametry procesu

Andrej Czan [1][*], Natalia Czanova [2], Ivan Kuric [3], Tatiana Czanova [4], Jozef Holubjak [5],

Andrej Czan [6], Dominik Krisak [7]

[1] Department of Machining and Production Engineering, Faculty of Mechanical Engineering - University of Žilina, Univerzitna8215/1, 010 26, Žilina, SLOVAKIA. E-mail: andrej.czan2@fstroj.uniza.sk

[2] Department of Machining and Production Engineering, Faculty of Mechanical Engineering - University of Žilina, Univerzitna8215/1, 010 26, Žilina, SLOVAKIA. E-mail: natalia.czanova@fstroj.uniza.sk

[3] Department of Automation and Production Systems, Faculty of Mechanical Engineering - University of Žilina, Univerzitna8215/1, 010 26, Žilina, SLOVAKIA. E-mail: ivan.kuric@fstroj.uniza.sk

[4] Department of Machining and Production Engineering, Faculty of Mechanical Engineering - University of Žilina, Univerzitna8215/1, 010 26, Žilina, SLOVAKIA. E-mail: tatiana.czanova@fstroj.uniza.sk

[5] Department of Machining and Production Engineering, Faculty of Mechanical Engineering - University of Žilina, Univerzitna8215/1, 010 26, Žilina, SLOVAKIA. E-mail: jozef.holubjak@fstroj.uniza.sk

[6] Department of Machining and Production Engineering, Faculty of Mechanical Engineering - University of Žilina, Univerzitna8215/1, 010 26, Žilina, SLOVAKIA. E-mail: andrej.czan@fstroj.uniza.sk.

[7] Department of Machining and Production Engineering, Faculty of Mechanical Engineering - University of Žilina, Univerzitna8215/1, 010 26, Žilina, SLOVAKIA. E-mail: dominik.krisak@fstroj.uniza.sk

[*] Corresponding author andrej.czan2@fstroj.uniza.sk

Streszczenie: SLS i MultiJet Fusion to technologie przyrostowe, które są jednymi z najczęściej stosowanych metod przetwarzania materiałów proszkowych do produkcji elementów polimerowych. Oferują wysoką elastyczność w tworzeniu złożonych i skomplikowanych komponentów, właściwości zbliżone do materiałów metalicznych oraz możliwość produkcji seryjnej. Głównym wymaganiem wobec tych technologii jest zapewnienie precyzji i dokładności w procesie wytwarzania. Jednak ze względu na różnice w procesach technologicznych, SLS i MJF różnią się istotnie, zwłaszcza w zakresie źródeł energii cieplnej wykorzystywanych do topienia materiału proszkowego oraz innowacyjnych metod wspierających konsolidację materiału. Te procesy także zapobiegają przepływowi ciepła, który mógłby wpływać na kontury komponentów. Do badań zastosowano jeden rodzaj proszku poliamidowego (PA 12) do produkcji próbek z użyciem technologii SLS i MJF. Eksperymentalna analiza próbek umożliwiła wstępne określenie twardości, co pozwala ocenić wpływ zastosowanej technologii na właściwości mechaniczne w postaci twardości. Następnie przeanalizowano dokładność wymiarową i kształtową wyprodukowanych próbek, co dostarczyło danych do oceny precyzji i dokładności zastosowanych urządzeń technologicznych. Dodatkowe eksperymenty skupiały się na analizie tekstury i precyzji powierzchni, w tym prostoliniowości, falistości i chropowatości. Podsumowując, zastosowane technologie SLS i MJF wykazują zarówno zalety, jak i wady, które należy monitorować, aby dokonać odpowiedniego wyboru technologii gwarantującej najlepszą dokładność i precyzję produkowanych komponentów..

Słowa kluczowe: twardość, właściwości mechaniczne, SLS, MJF

1. Introduction

One of the most applied additive technologies is powder material fusion (PBF) processes, which are a subset of additive manufacturing (AM) techniques that involve the subsequent layering of materials in powder form and the use of an energy source to melt particles in selected areas of the powder base.[1] Based on the type of heat source and process material, we distinguish between different PBF production process techniques.[2] Selective laser sintering (SLS) and Multijet fusion (MJF) are the most widely used techniques for processing polymer components.[2]

As confirmed by the global trade statistics published in Wohlers' 2022 report, the polymer powder market has grown by 43% in the past year, surpassing photopolymer resins as the most widely used AM material to date.[3] This

knowledge points to the significant impact of additive manufacturing thermo-polymers on an industrial scale. All PBF thermos-polymer techniques can be described in three main steps.[4] First, the base plate is gradually preheated to a temperature just below the start of polymer melting, and the powder material is homogeneously distributed in a thin layer. Subsequently, the heat source induces the melting of particles in the real area of the powder primer according to a 3D computer-aided design (CAD). The consolidation of the new layer and its fusion with the previous layer takes place through coalescence and gradual solidification of the material. After applying a new layer, the foundation slab is lowered by the height of the layer, and these steps are systematically repeated until the production of the 3D model is completed.[4]

The first additive PBF technology for industrial applications was SLS, the first commercialized process, developed in the late 1980s at the University of Texas,[1] and is currently one of the most widely used AM methods for processing thermos-polymer based materials. In addition to the main advantages typical of additive manufacturing processes, such as the ability to produce fully customized complex-shaped and articulated parts without the need for production molds and tools, or the avoidance of waste production for secondary processing, the high dimensional flexibility, accuracy, and good properties of SLS parts, as well as the growing selection of available materials, are moving towards attractive technologies on an industrial scale, especially for aerospace, automotive, medical or tool industry.[5,6] Due to the preheating of the material in the bed, PBF technologies do not require support structures for the production of components, nor for overhanging or negative elements or thin walls. These properties make it possible to increase the saturation of the space of the construction chamber, which enables large-scale production of thermos-polymer components.[6]

As an alternative to SLS technology, MJF technology has been developed in the last decade. MJF technology was patented in 2014 and brought to reality in 2016 by Hewlett-Packard Inc. (HP), the technology works with very similar procedures to SLS but differs significantly in the application of the energy heat source and the material consolidation mechanism.[1] SLS technology uses a laser beam to selectively combine thermos-polymer particles; the power source is coherent and focused by galvanometric mirrors and lenses on a layer of powder to follow the contour of each scanned cross-section of the object.[6] Generally, CO_2 laser is used, due to the absorption of polymeric materials at the corresponding wavelength of $10.6\mu m$ is high.[1] MJF technology involves the application of a series of infrared (IR) lamps that move over a layer of thermos-polymer powder previously impregnated with a printing binder at the voxel level.[7] The ink heads apply the binder to selected areas of the powder layer corresponding to the cross-section of the part and the detailed agent along its contour.[7] The interaction of infrared radiation with the impregnated powder material promotes material consolidation due to the specific role of the deposited binder and reagent. A curing agent is an IR-absorbing ink that contains an aqueous solvent, soot, and other organic additives. Carbon black acts as an IR-absorbing compound that converts incoming IR radiation into thermal energy, causing powders to melt.[8,9] A detailing agent serves to inhibit the fusion of powders surrounding parts by providing a local cooling effect based on solvent evaporation and improving manufacturing resolution and accuracy.[8,9]

In the MJF process, infrared lamps deliver an evenly distributed energy input over the entire build plate, causing the melting of selected areas of the powder bed where fixing agents are applied. SLS laser technology selectively scans the area layer by layer.[10] The process has a major disadvantage because the layering speed is limited to 1200 cm3h-1 with a maximum laser scanning speed of 5 m.s-1[10,11] and the production time largely depends on the cross-sectional size of the printed parts.[12] Compared to the SLS, MJF technology has a rapid movement across the construction plane where the infrared lamps and ink heads are located, ensuring that the powder material is melted evenly, allowing for a geometry-independent layer processing time of approximately 10 seconds.[10] The process of multijet technology significantly reduces the processing time due to the time-consuming SLS laser sintering method, as the assembly speed can reach up to 5058 cm3h-1.[13] MJF technology represents a progressive alternative for the processing of powdered thermos-polymer materials. Comparing SLS and MJF technologies is important to evaluate the performance differences between the respective parts and to make the right choice of process. In addition to the different energy source of heat and the consolidation mechanism, the compared processes also differ in the layering mechanism, where in SLS technology it is a blade and in MJF it is a rotating cylinder and there is also a different temperature of the powder bed.[12]

Among the relatively limited range of materials available for processing with SLS, polyamide 12 (PA12), a thermoplastic polymer with a semi-crystalline structure, is certainly the most widely used and researched.[5,6] The use of a power source such as a CO_2 laser or infrared lamp causes the powder part to melt; the low viscosity of the melt leads to a high coalescence rate and high compaction of the material.[5,6] Most of the research work on MJF technology has focused on the pure polymer PA12 and has studied various aspects such as mechanical properties,[14–18] surface quality,[10,12,19] powder aging,[20] the role of inks [21,22] and cooling rates[23,24]. To compare the produced samples obtained by SLS and MJF technologies, PA12 was selected as a reference material. Sillani et al.[12] The properties of raw materials and components produced by these two technologies were thoroughly examined. For this purpose, the commercially available material PA12 was used and two commercially available technologies SLS and MJF were

compared. It has been found that the properties of the powder material, such as particle size and shape distribution, thermal transitions, and phase composition, are similar for the two powder systems; however, differences were observed in the fraction of fine particles, as well as in the recyclability of powders (due to the end coating of polymer chains in the MJF raw material).[12] With regard to manufactured components, anisotropy was reported when changing the print orientation from the assembly plane (i.e. *XY*) on the Z axis. The similarities and differences between the SLS and MJF techniques in terms of raw powders and the properties of the final parts have also been proven by other authors.[10:25–27] Xu et al.[10] suggested that the higher heating ability of the laser source compared to IR lamps induces higher melting efficiency in SLS, resulting in lower pore content and excellent rigidity and strength of parts manufactured in the construction plane (i.e., XY).[10] Rosso et al. [25] found that the elongation at rupture of MJF specimens is significantly higher compared to SLS counterparts. Cai et al.[26] confirmed that both techniques produce anisotropic parts as a function of deposition orientation, with the SLS process being more susceptible to this effect. Among the three main axes, the highest variation in mechanical properties was recorded in the *Z orientation*, where the tensile strength of MJF samples is 25% higher.[26] Calignano et al. [27] attributes this large difference to the flux effect, resulting in less volume and the number of elongated pores for parts of the MJF.

However, most of the literature starts with two different powders for sample making using SLS and MJF and then compares their final properties.[10,12,25–28] In contrast, this work provides a thorough comparison between two different technologies, as the samples were produced using the same PA12 powder material, nominally designed for MJF and directly supplied by HP. The samples were then characterized by the same set of experimental analyses. This approach allows us to clearly distinguish the influence of the different processing conditions and consolidation mechanisms that occur in SLS and MJF on the performance of the parts. Since a review of the literature has indicated that the variation of mechanical properties with the orientation of the part is a critical factor for the potential applications of each technique, this aspect will be central to this study.

In their paper (12), the authors M. Mele, G. Campana, G. L. Monti designed and applied a sample model that is oriented in the XY plane with the orientation directions themselves according to Table 1. The model was applied to the MJF process. The direction in which the UV lamps moved was shown along the X-axis, while *the Y-axis* determines the direction of movement of the detailing nozzles.
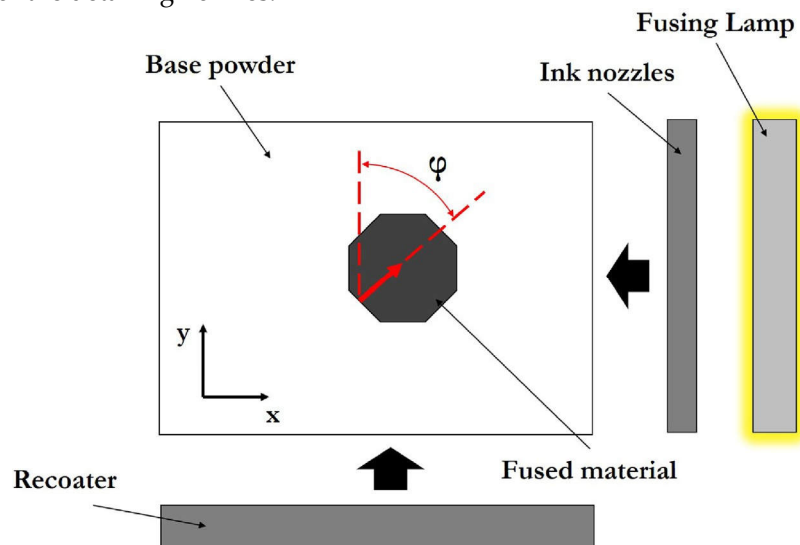
Figure 1. Orientation of a generic border edge of the benchmark geometry with respect to the Y-axis (12)

The reference model was a thin octagon to observe and measure the capillarity effect at the edge edges with different orientations in relation to the *XY plane* within the building platform Fig. 1 a. Fig.2 shows the orientation of the reference part within the construction platform of the 3D printer and the angle of φ between the normal direction of the contained edge and the Y-axis of the machine. Each edge is then identified by the angle φ and especially the following correspondences were applied in the experimental and modeling activity (Table 1). The thickness of the reference value along the Z-axis has been set to the same value of 5.0 mm to achieve adequate part rigidity and thin geometry, resulting in a negligible shrinkage effect.

Figure 2. Benchmark geometry, a manufactured benchmark part (upper surface), and map of deviations of the upper surface along the Z-axis. (12)

Table 1. Orientation of the border edge of the benchmark geometry.(12)

φ (Rad)	Direction (–)	Label (–)
0	South	S
π/4	South-East	SE
π/2	East	E
3π/4	North-East	NE
π	North	N
5π/4	North-West	NW
3π/2	West	W
7π/4	South-West	SW

On a given sample model, it is possible to identify dimensional and shape accuracy only in the XY plane, or YZ or XZ, which does not provide a comprehensive spatial evaluation of geometric accuracy. In order to be able to comprehensively evaluate the geometric accuracy of the technological equipment, it is necessary to design a sample that will respect the XYZ orientation as well as the positive and negative inclination to the based board.

2. Experimental Section

2.1. Material and Technology Equipment

PA12 powder material was purchased from Hewlett-Packard (Palo Alto, CA, USA) under the trade name HP 3D PA 12. The powder material was processed using both MJF and SLS technologies to compare the hardness and accuracy of the samples produced derived from two different PBF processes. Sinterit Lisa laser sintering machines were used to process SLS and MJF as A and HP Jet Fusion Series 5210 powder technology (Hewlett-Packard, Palo Alto, CA, USA). The Sinterit Lisa printer uses a continuous CO2 laser with a diameter of 200 μm (λ = 10.6 μm) to selectively melt polymer powders deposited in successive thin layers with a translational blade on the build plate (Figure 2a). The powders are preheated by two halogen lamps located above the build plate throughout the construction process. During the production of each layer, the laser scans the circuitry of the objects before hatching the internal areas.[31]

The process parameters for SLS parts have been optimized to minimize the porosity content and prevent the deformation of the parts. The temperature of the powder bed has been set at 171 °C, as lower values cause the structure to fail due to the corrugation of the part. The laser power (P), scan speed (v), and scan pitch (s) have been set to 6.3 W, 2400 mm s-1, and 100 μm. The height of the layer (h) was also set to 100 μm. The volume energy density of the laser (ED),[1] equal to 0.263 J mm-3 for the optimized parameter sets was calculated according to equation (1):

$$ED = \frac{P}{v.s.h} \tag{1}$$

The HP Jet Fusion Series 5210 Printer consists of a design unit in which powders are spread with a roller to form a thin layer of solid thickness and a movable transport unit containing a series of dual-agent printheads and two sets of IR fuser lamps on either side.[7] The trolley unit moves across a construction platform, preheated to a fixed temperature

by a ceiling infrared lamp positioned above the print bed to selectively apply patented fixing and detailing agents inside and outside the boundaries of the part. These agents are dispensed from a series of thermal inkjet nozzles in a discreet manner with high spatial resolution.[8] IR lamps cause selective melting of powders in areas where a binder has been applied, while detailed ink prevents heat transfer outside the molten area by evaporation.[7,8] The build plate is then moved downward by a distance equal to the thickness of the layer to allow the cylinders to spread the new powder layer. These steps are repeated repeatedly until the part is completed.[7,8] A diagram of the MJF process just described is outlined in Figure 2b.

For the MJF technique, a single printing mode available for processing high-reusability PA12 3D powders was adopted, consisting of two print passes at a speed of about 10s per layer.[29,30,32] However, HP does not disclose details of process parameters (e.g., irradiation and lamp speed) for intellectual property reasons.[25,33] The layer height was set to 80 µm as recommended by the printer manufacturer.

Both machines operate in an airborne environment. The effective print volume of the Sharebot SnowWhite2 (150 x 200 x 150 mm) is significantly smaller compared to the HP Jet Fusion Series 5210 (380 x 284 x 380 mm[13]) or other industrial SLS machines.[34] This difference in chamber sizes could affect the thermal history and cooling time of the samples at the end of the printing process.

(a)   (b)
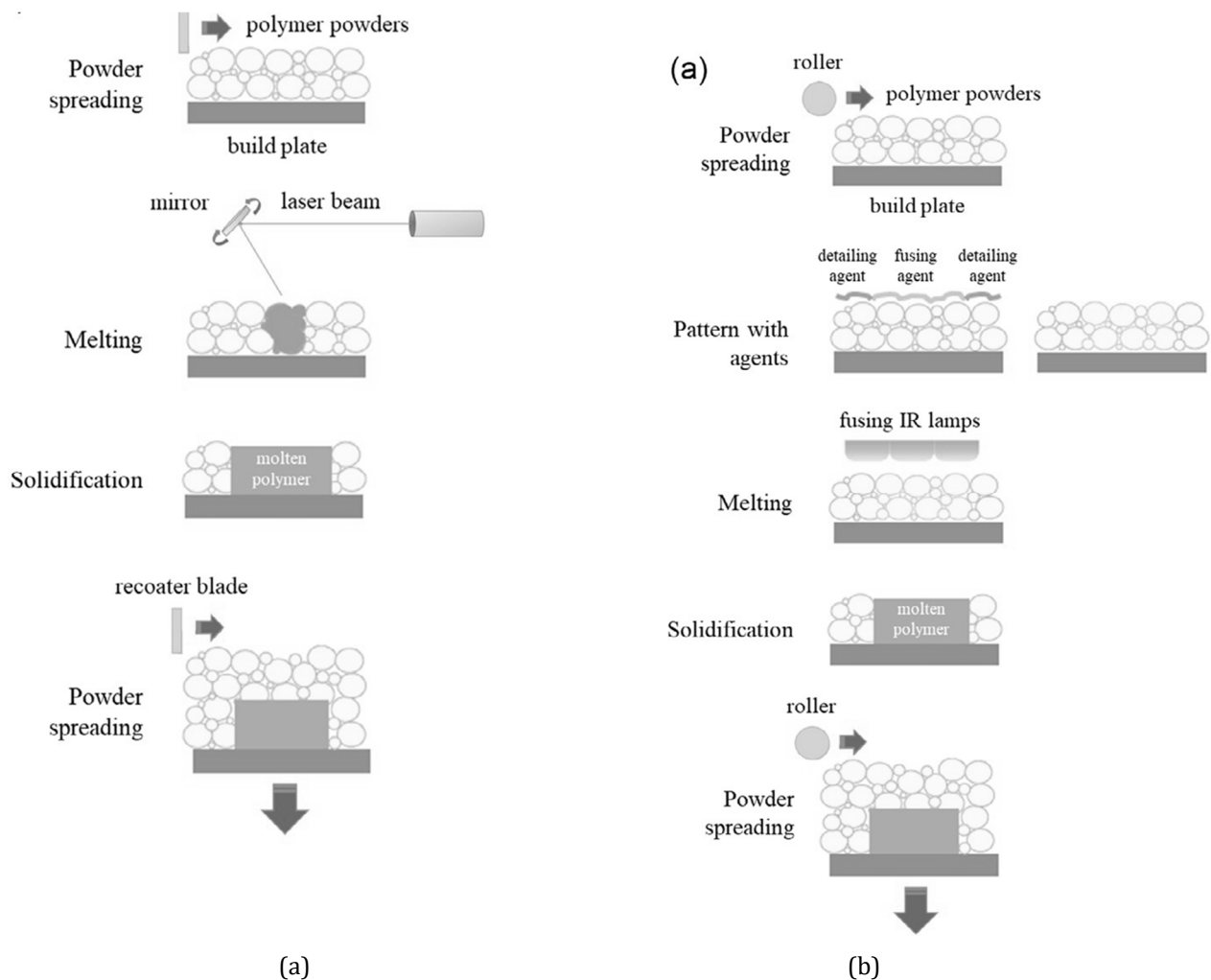
Figure 3. Schematic representation of the principle of operation of the two investigated PBF processes: a) SLS and b) MJF

The design foundation of the experimental sample is centered on creating reference areas aligned with the X, Y, and Z coordinate systems. Given the application of additive manufacturing (AM) technologies, it is evident that the formation of layers and their properties post-curing exhibit variability. This variability is affected by the sample's orientation within the building chambers along the X, Y, and Z axes, as well as the direction in which the layers are applied. Previous research and experience have produced numerous reference samples for comparative monitoring and

detailed object creation in AM technologies. However, these samples do not account for the effects of specific orientations or the layering directions of 3D models.

To facilitate comprehensive volume or spatial analysis in three-dimensional orientation, it is essential to design the sample to encompass all orientations, including both positive and negative angles in the Z orientation. Consequently, the sample was crafted in a three-dimensional format, featuring octagonal areas where all faces are equidistant and parallel to one another, as illustrated in Figure 4. Each parallel face maintains a distance of 60 mm, with hole samples designed with a 10 mm diameter and threaded samples featuring an M10 thread.
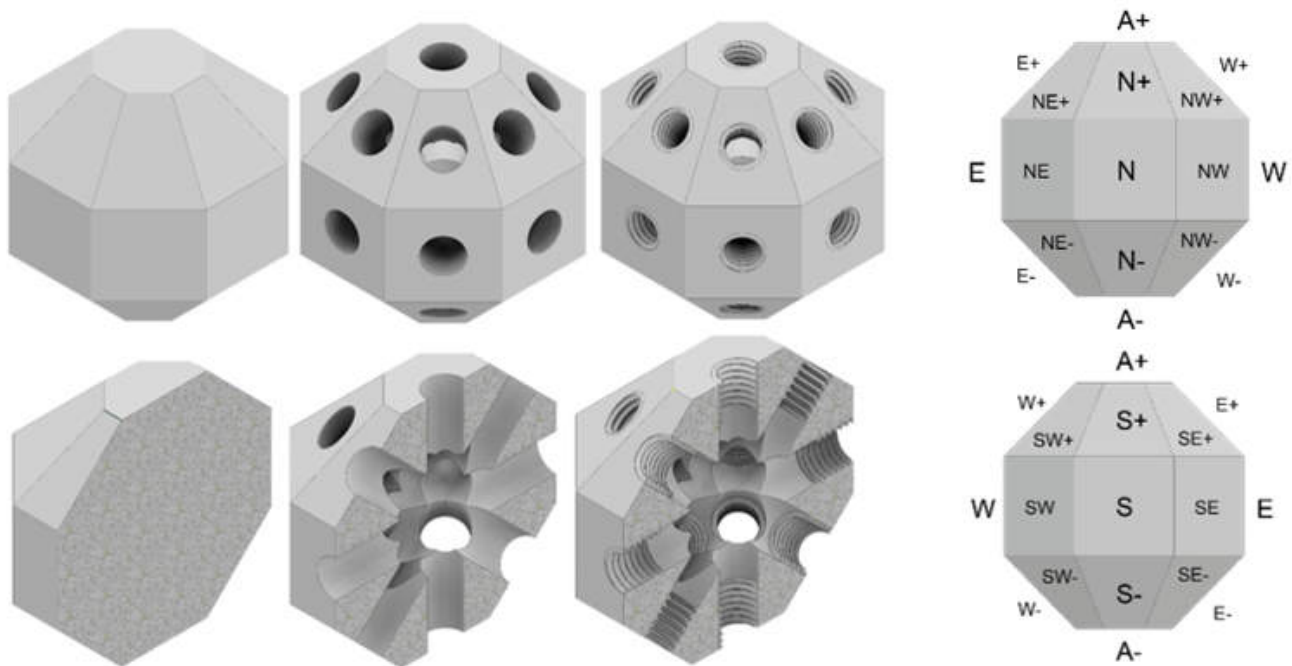
Figure 4. displays 3D models of samples in their complete form (P), featuring holes (D) and threads (Z). Additionally, it includes a detailed view of the samples in section, highlighting the NSEW+/-A marking system for the monitored areas on the right.

The sample design features eight square sections on the XY plane. In the Z direction, there are two parallel octagonal faces, designated as areas with positive and negative inclinations. The surfaces that connect the square and octagonal areas create trapezoidal surfaces, each sloping either positively or negatively. Altogether, the sample consists of 26 parallel surfaces, forming a 26-sided shape resembling a Revolved Sphere. The proposed samples allowed for accurate identification of working precision, facilitating the analysis of dimensional specifications, shape characteristics, and surface roughness.

2.2. Characterization techniques

Real samples were fabricated according to the design specifications, featuring a complete shape with integrated holes and threads created during the layering process. These samples were oriented using the Cartesian coordinate system illustrated in Figure 4. To simplify the complex spatial quadrant designation, a more straightforward coordinate system was adopted: the X-axis as East-West (E-W), the Y-axis as North-South (N-S), and the Z-axis as Above-Below (A+ and A-). The samples exhibit eight square faces in the XY plane, labeled according to cardinal and intercardinal directions (N, S, E, W, NE, NW, SE, SW), as well as A+ and A- for the vertical dimension. In the Z orientation, two parallel octagonal faces are present, designated as A+ (positive inclination) and A- (negative inclination). This marking system was implemented to facilitate the identification of distinct areas on a spherical object. Utilizing this labeling scheme, samples were produced at various stations of the manufacturing equipment. Figure 5 presents samples manufactured using Selective Laser Sintering (SLS) technology, while Figure 6 showcases objects created with Multi Jet Fusion (MJF) technology.

Figure 5. Realistically created identification experimental samples and their three variants plan P, with holes D and threads Z produced by SLS technology

Figure 6. Realistically created identification experimental samples and their three variants plan P, with holes D and Z threads produced by MJF technology

To determine the surfaces created during the process and evaluate their fundamental parameters—directness (P), roughness (R), and corrugation (W)—we utilized the Infinite Focus G5 device. This advanced system offers a comprehensive solution by combining the optical measurement of micro-coordinates with surface treatment analysis. Renowned for its precision, speed, and flexibility, the Infinite Focus G5 is a state-of-the-art optical 3D measurement system tailored for diverse surface assessment needs.

The G5 system merges the capabilities of a 3D micro-coordinate measuring machine with those of a surface roughness measurement device, creating a versatile two-in-one solution. This dual functionality enables the precise measurement of various surface types and properties. When working with micro-precision components, the system assesses all relative surface characteristics using a single, multifunctional measurement sensor. It delivers highly accurate, consistent, and repeatable results, achieving a remarkable vertical resolution of up to 10 nanometers (nm).

The system's measurement principle is based on hardware-assisted vibration damping and focus variation technology. This innovative approach facilitates the detailed analysis of both the shape and surface roughness, even for large and heavy objects. The Infinite Focus G5 is equipped with built-in, high-precision positioning devices along its X and Y axes, ensuring exceptional accuracy during lateral movements. This capability is crucial for thorough and precise surface mapping. Moreover, its automated interface supports fully automatic measurements, making it an ideal tool for deployment in production environments where efficiency and consistency are critical.

The scanned areas evaluated at position 'S' are depicted in Figure 7, showcasing the detailed analysis and capabilities of the Infinite Focus G5. This robust system ensures reliable results across a wide range of applications, making it indispensable for surface characterization tasks.
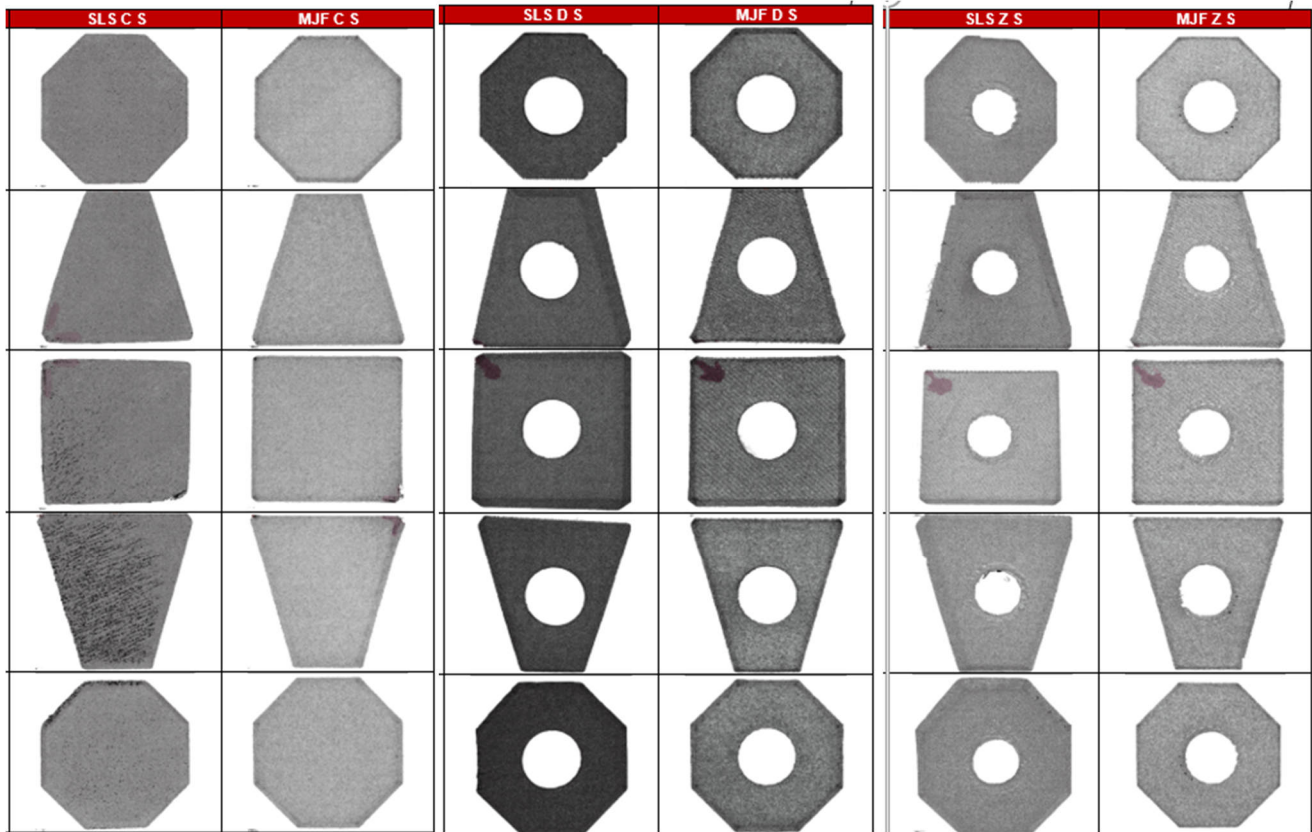
Figure 7: Scanning images of the surfaces in the "S" position for experimental samples of solid P, which include holes D and Z threads

2.3. Evaluation of surface parameters P, R, and W

The primary mean arithmetic deviation of the profile was observed, which is considered, in our case Pa, Ra, Wa is determined as the mean arithmetic value of the absolute deviations of the profile Z(x) in the range of their basic length [22,24,29].

$$Pa, Ra, Wa = \frac{1}{l} \int_0^l /Z(x)/dx \ , \ for \ l = lp, lr \ or \ lw \quad [mm] \tag{2}$$

The mean quadratic deviation of the considered profiles in our case profiles Pq, Rq, and Wq is determined as the mean quadratic value of the absolute deviations of the profile Z(x) in the range of their base length. [22,24,29]

$$the \ Pq, Rq, Wq = \sqrt{\frac{1}{l} \int_0^l Z(x)^2 \, dx} \ , \ \mathbf{for} \ l = lp, lr \ or \ lw \quad [mm] \tag{3}$$

The total height Pz, Rz, Wz, is the sum of the maximum height of peak Zp and maximum depression Zv of the profile within the assessment length, not the sampling length. The Rt≧Rz relationship applies to all profiles. Pt Maximum total section height and Wt Maximum total corrugation height [22,24,29].

$$Pz, Rz, Wz = maxZp + maxZv \ , \ \mathbf{for} \ l = lp, lr \ or \ lw \quad [mm] \tag{4}$$
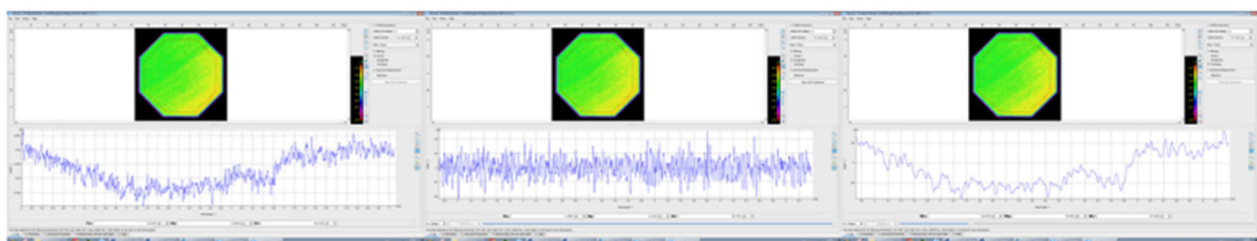
Figure 8 Model of evaluated surfaces for full sample and area A+, parameters Ra, Rq, and Rz identified

The device was configured to analyze samples, scanning the surfaces produced by SLM and ADAM technologies in three forms: a full sample (P), a hole model (D), and a threaded model (Z). For each sample, the areas A+, S+, S, S-, and A- were scanned to assess the surface from different orientations. A sample of the scanning results is presented in Fig. 8. The parameters evaluated include Pa, Ra, Wa, Pq, Rq, Wq, Pz, Rz, and Wz. A comparison of the scanned surfaces for all three types of experimental samples is illustrated in the color map analysis shown in Fig. 9.
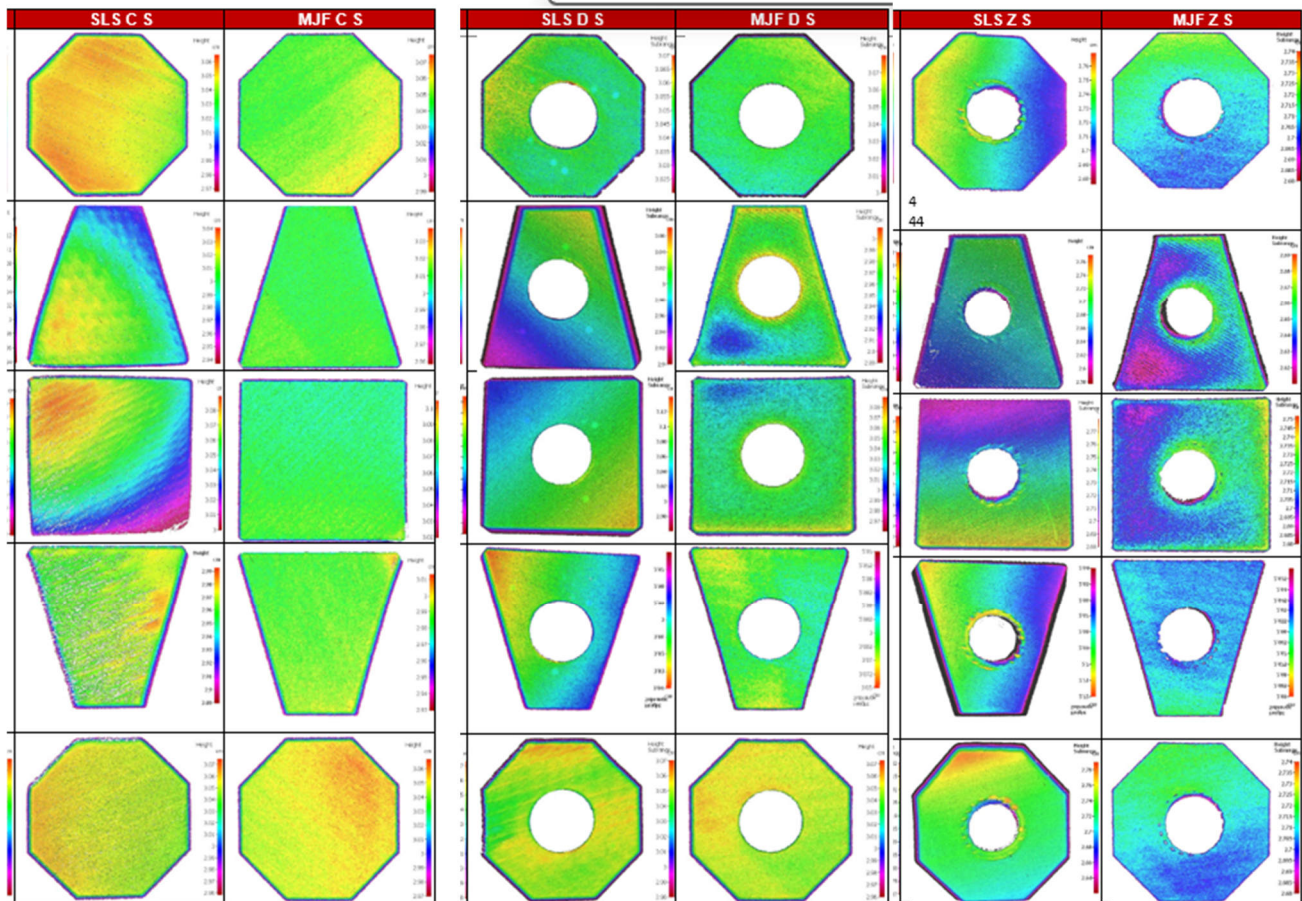
Figure 9: Images of the scanned surfaces in the "S" position, featuring texture identification through a color map for experimental samples of solid P, including holes D and Z threads

2.4. Methodology for Evaluating Working Accuracy

The purpose of the working accuracy analysis is to assess the dimensional and shape accuracy achievable through the ADAM process. This analysis utilized reference samples specifically designed to identify the fundamental precision characteristics of additive manufacturing (AM) processes. The reference part comprises simple geometries of varying dimensions that represent the accuracy across the first eight ranges of basic size and parallelism of each face, as shown in Fig. 4. Dimensional and geometric tolerances, including shape defects, were evaluated for both convex and concave features of the artifact according to the established system.

The assessment of the dimensional accuracy of the replica was conducted in accordance with Directive ISO 286-1:1988. For each ISO base size range, the dimensional accuracy of the ADAM process was evaluated in relation to the achieved IT level of the replica artifact. Specifically, the IT precision level was defined by considering the maximum dimensional error as the number of unit tolerances n corresponding to the 95th percentile of the distribution of unit tolerances nj for the general jth dimension, where nj is calculated as follows:

$$n_j = \frac{1000|D_{jn} - D_{jm}|}{i} \tag{5}$$

where D_{jn} represents the nominal dimension, D_{jm} denotes the actual dimension of the feature, and i is a tolerance factor that varies across different ranges of the basic ISO size (see Table 2).

Table 2. Basic size ranges and corresponding tolerance factors ii as defined by the International Organization for Standardization (ISO)

Range		Basic Size							
Above D_1 (mm)		1	3	6	10	18	30	50	80
Up to including D_2 (mm)		3	6	10	18	30	50	80	120
Standard tolerance factor i (µm)		0.542	0.733	0.898	1.083	1.307	1.561	1.856	2.173

The actual dimension is calculated as the average of three measurements of a single geometric feature of the replica. Measurements were conducted using the Zeiss Eclipse coordinate measuring machine (CMM), specifically the GLOBAL Image 07.07.07 model, which has a declared maximum permissible error (MPEE) of 2.2 µm + $L/1000$ in accordance with ISO-10360/2, where L is the measured length. Table 3 presents the classification of dimensional quality, as ISO IT grades are dependent on n.

Table 3. Classification of IT levels as per ISO 286-1:1988.

Range		IT 10	IT 11	IT 12	IT 13	IT 14	IT 15	IT 16
Above 1 mm	Up to 500 mm	64i	100i	160i	250i	400i	640i	1000i

3. Results and discussion

Hardness was identified using the Leeb HLD method, SLS and MJF technology, where the experiment was oriented to measure hardness on surfaces A+, S+, S, S-, A-. The measurement also consisted of three measurements and the subsequent average of the measured HLD hardness values. The hardness was measured and then compared based on the different shape of the 3D model P, D and Z, as well as on the basis of different AM technologies. The hardness for individual shapes of the 3D models was of different hardness even for individual surfaces of the sample itself. The change was observed on A+ surfaces with A- compared to other surfaces where the highest hardness values were recorded, but also as differences between A+ and A- with SLS technology. When comparing different shapes, you can see the difference in hardness at holes and threads, which is different from the P-shape. With the P-shape, the hardness has a minimal change in hardness. Figure 10.
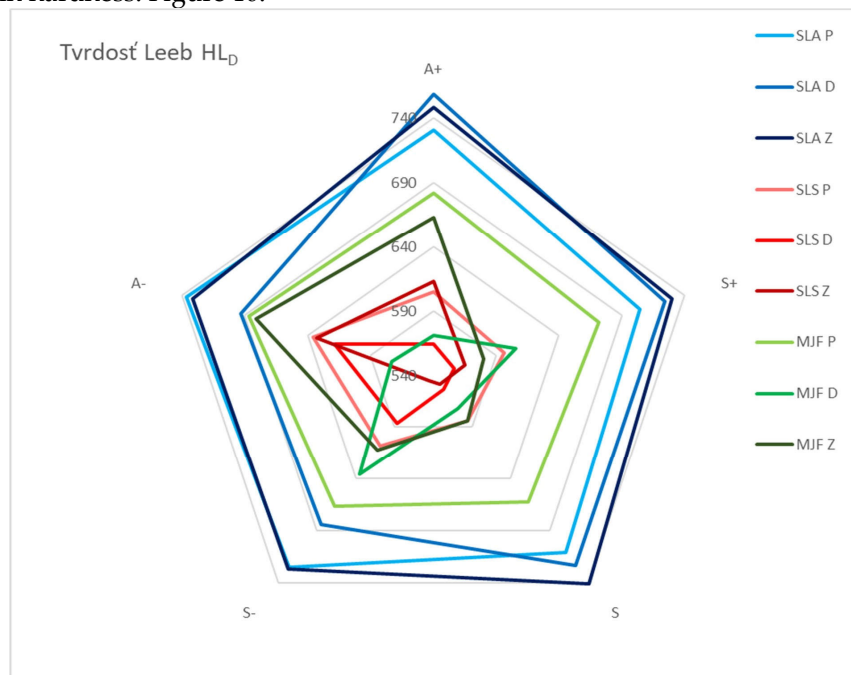
Figure 10 Comprehensive comparison of average Leeb HLD hardness values for the analyzed SLA, SLS, MJF technologies and individual samples P, D and Z

The comparison of the achieved data from the experimental measurement can also be seen in the comprehensive comparison of applied AM technologies, where the difference in the size of the measured hardness values can be seen, where lower values were recorded in SLS samples that have significant changes in hardness. Higher values were obtained for MJF samples, which are higher by about 12-15%, but a difference is found between the hardness depending on the shape of the 3D model.

After scanning the individual surfaces with the InfiniteFocus G5 optical measuring device, a summary comparison of the achieved surface parameters was conducted. The results allowed for a comparison of the solid P model with holes D and threads Z for a single technology, enabling the assessment of how the technology and the shapes of models P, D, and Z influenced the resulting areas in various orientations: A+, S+, S, S-, and A-. The results were then compared across different technologies regarding surface properties. Figures 11 to 16 present the measured deviations, their average values, and the standard deviation, along with a graphical polar display.

From the graphs, it can be concluded that the sample produced using Binder Jetting technology exhibited the best values among the examined samples. The sample created with MJF technology achieved the highest values for the Full Sample. In contrast, SLS technology yielded the least satisfactory results due to the presence of support structures, which require additional processing for removal.

AREA	IT rozsah min. [mm]	IT rozsah priem. [mm]	IT rozsah max. [mm]	ITx min	ITx averg	ITx max
A1/A2	84	62	37	IT11	IT10	IT9
N/S	114	24	100	IT11	IT8	IT11
NW/SE	289	275	259	IT13	IT13	IT13
W/E	207	187	153	IT13	IT12	IT12
SW/NE	281	234	187	IT13	IT13	IT12
N+/S-	333	205	126	IT14	IT12	IT11
N-/S+	421	390	365	IT14	IT14	IT14
NW+/SE-	346	168	63	IT14	IT12	IT10
NW-/SE+	362	350	323	IT14	IT14	IT14
W+/E-	393	357	326	IT14	IT14	IT14
W-/E+	208	175	93	IT13	IT12	IT11
SW+/NE-	304	260	211	IT13	IT13	IT13
SW-/NE+	351	331	294	IT14	IT14	IT13
average	284	232	195	IT13	IT13	IT12
min	84	24	37	IT11	IT8	IT9
max	421	390	365	IT14	IT14	IT14
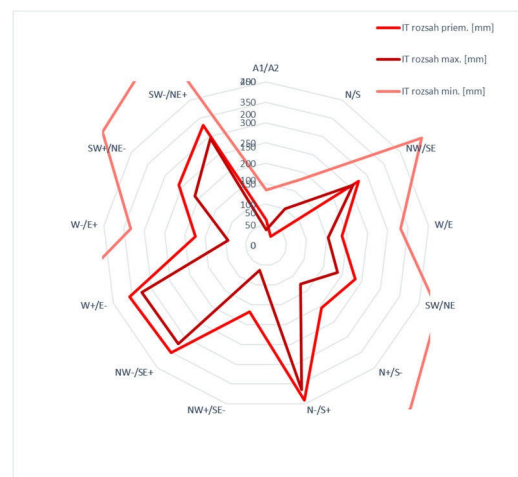
Figure 11. Summarization of values from measurements for SLS technology full P sample shape and their graphical comparison in polar view

AREA	IT rozsah min. [mm]	IT rozsah priem. [mm]	IT rozsah max. [mm]	ITx min	ITx averg	ITx max
A1/A2	109	85	50	IT11	IT11	IT9
N/S	155	63	188	IT12	IT10	IT12
NW/SE	117	40	38	IT11	IT9	IT9
W/E	60	31	4	IT10	IT8	IT0-4
SW/NE	205	71	269	IT12	IT10	IT13
N+/S-	276	181	143	IT13	IT12	IT12
N-/S+	366	145	14	IT14	IT12	IT7
NW+/SE-	180	111	87	IT12	IT11	IT11
NW-/SE+	265	245	232	IT13	IT13	IT13
W+/E-	193	173	143	IT12	IT12	IT12
W-/E+	218	148	106	IT13	IT12	IT11
SW+/NE-	348	156	59	IT14	IT12	IT10
SW-/NE+	188	140	91	IT12	IT12	IT11
average	206	122	110	IT13	IT11	IT11
min	60	31	4	IT10	IT8	IT0-4
max	366	245	269	IT14	IT13	IT13
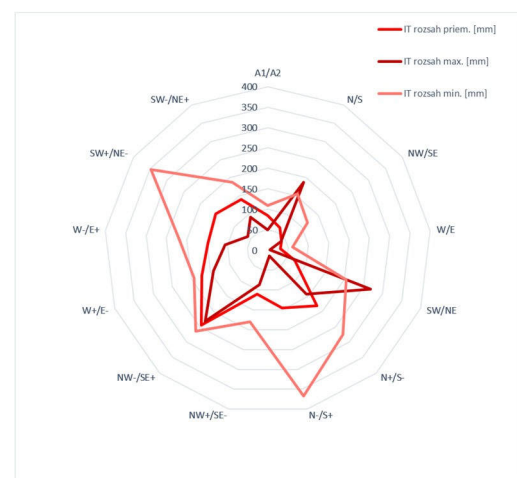
Figure 12. Summarizing the values from measurements for SLS technology, the shape of the D-hole sample and their graphical comparison in polar view

AREA	IT rozsah min. [mm]	IT rozsah priem. [mm]	IT rozsah max. [mm]	ITx min	ITx averg	ITx max
A1/A2	76	20	119	IT10	IT7	IT11
N/S	111	69	205	IT11	IT10	IT13
NW/SE	55	14	145	IT10	IT7	IT12
W/E	197	93	27	IT12	IT11	IT8
SW/NE	317	74	107	IT13	IT10	IT11
N+/S-	154	76	6	IT12	IT10	IT5
N-/S+	372	257	186	IT14	IT13	IT12
NW+/SE-	150	75	2	IT12	IT10	IT0-4
NW-/SE+	339	254	186	IT14	IT13	IT12
W+/E-	203	157	60	IT12	IT12	IT10
W-/E+	378	286	74	IT14	IT13	IT10
SW+/NE-	321	126	37	IT14	IT11	IT9
SW-/NE+	385	307	189	IT14	IT13	IT12
average	235	139	103	IT13	IT12	IT11
min	55	14	2	IT10	IT7	IT0-4
max	385	307	205	IT14	IT13	IT13
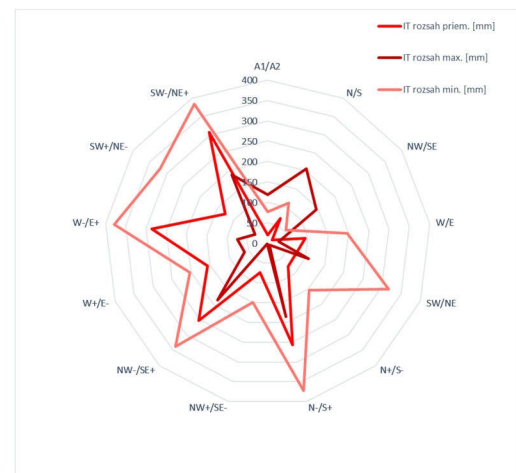
Figure 13. Summarizing the values from measurements for SLS technology, the shape of the sample with Z threads and their graphical comparison in the polar view

AREA	IT rozsah min. [mm]	IT rozsah priem. [mm]	IT rozsah max. [mm]	ITx min	ITx averg	ITx max
A1/A2	83	51	5	IT11	IT9	IT0-4
N/S	38	7	56	IT9	IT5	IT10
NW/SE	110	79	43	IT11	IT10	IT9
W/E	23	85	201	IT8	IT11	IT12
SW/NE	69	86	113	IT10	IT11	IT11
N+/S-	433	385	344	IT14	IT14	IT14
N-/S+	136	106	76	IT12	IT11	IT10
NW+/SE-	307	262	189	IT13	IT13	IT12
NW-/SE+	133	119	107	IT12	IT11	IT11
W+/E-	206	168	134	IT13	IT12	IT12
W-/E+	152	140	117	IT12	IT12	IT11
SW+/NE-	90	44	3	IT11	IT9	IT0-4
SW-/NE+	239	212	157	IT13	IT13	IT12
average	155	134	119	IT12	IT12	IT11
min	23	7	3	IT8	IT5	IT0-4
max	433	385	344	IT14	IT14	IT14
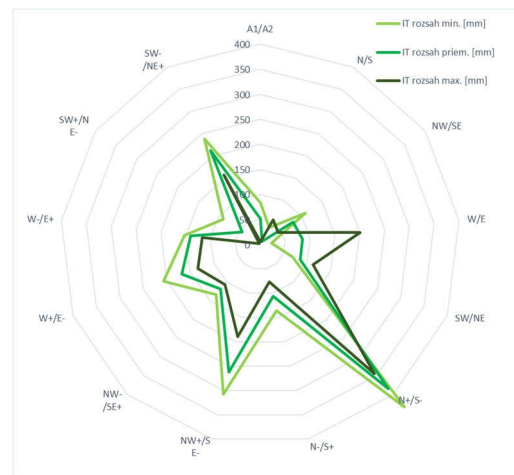
Figure 14. Summarizing the values from measurements for MJF technology full P sample shape and their graphical comparison in polar view

PLOCHA	IT rozsah min. [mm]	IT rozsah priem. [mm]	IT rozsah max. [mm]	ITx min	ITx priem	ITx max
A1/A2	92	64	29	IT11	IT10	IT8
N/S	106	60	15	IT11	IT10	IT7
NW/SE	23	16	36	IT8	IT7	IT9
W/E	36	19	1	IT9	IT7	IT0-4
SW/NE	203	148	83	IT12	IT12	IT11
N+/S-	174	162	151	IT12	IT12	IT12
N-/S+	370	317	268	IT14	IT13	IT13
NW+/SE-	188	164	141	IT12	IT12	IT12
NW-/SE+	215	172	138	IT13	IT12	IT12
W+/E-	280	235	211	IT13	IT13	IT13
W-/E+	147	139	129	IT12	IT12	IT11
SW+/NE-	417	357	280	IT14	IT14	IT13
SW-/NE+	180	147	123	IT12	IT12	IT11
priemer	187	154	123	IT12	IT12	IT11
min	23	16	1	IT8	IT7	IT0-4
max	417	357	280	IT14	IT14	IT13
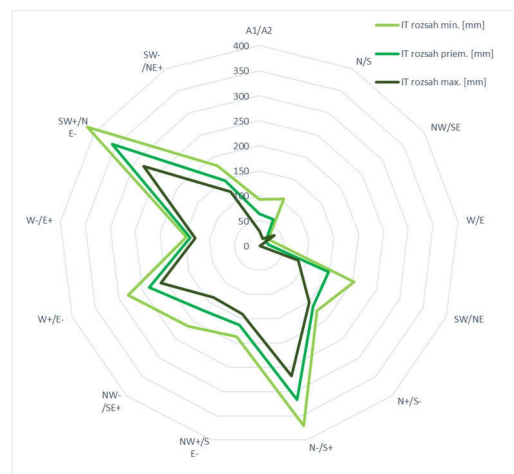
Figure 15. Summarizing the values from measurements for MJF technology, the shape of the D-hole sample and their graphical comparison in the polar view

AREA	IT rozsah min. [mm]	IT rozsah priem. [mm]	IT rozsah max. [mm]	ITx min	ITx priem	ITx max
A1/A2	114	69	27	IT11	IT10	IT8
N/S	118	75	3	IT11	IT10	IT0-4
NW/SE	19	5	15	IT7	IT0-4	IT7
W/E	46	3	32	IT9	IT0-4	IT8
SW/NE	75	46	28	IT10	IT9	IT8
N+/S-	193	179	169	IT12	IT12	IT12
N-/S+	302	242	179	IT13	IT13	IT12
NW+/SE-	197	179	163	IT12	IT12	IT12
NW-/SE+	223	193	162	IT13	IT12	IT12
W+/E-	240	217	185	IT13	IT13	IT12
W-/E+	210	172	140	IT13	IT12	IT12
SW+/NE-	302	261	218	IT13	IT13	IT13
SW-/NE+	216	172	129	IT13	IT12	IT11
priemer	173	139	112	IT12	IT12	IT11
min	19	3	3	IT7	IT0-4	IT0-4
max	302	261	218	IT13	IT13	IT13

Figure 16. Summarizing the values from measurements for MJF technology, the shape of the sample with Z threads, and their graphical comparison in the polar view

By analyzing the data obtained to monitor the working accuracy of AM technological devices, it is possible to observe very interesting results that select the importance of the technology and its character.

By observing the data from Fig. 14-16, the influence of MJF technology on the accuracy can be seen, which ranges between IT5-IT10 in the Z shape and in the D and P shape around IT10-IT13. Very interesting is the minimal difference in IT working accuracy when looking at the overall sample view, where there is a significant disproportion with SLS technology, which is also visible in the graphic display as a comprehensive view of the working accuracy of the samples produced. The disproportion is expressed by the distinctive shape of the star-shaped graphic representation of the data, which indicates the instability of repeatability or precision of the process. However, the working accuracy is better than with SLS technology, and the best accuracy and precision of the process were found with MJF technology.

4. Conclusion

The study systematically compared two industry-relevant polymer PBF techniques, SLS and MJF, by examining the thermophysical properties of the raw material (i.e. the same PA12 powder), where the basic technological characteristics were compared. The study analyzed the current state of additive manufacturing using plastic materials with regard to the quality and quantity of the production process. Based on the analysis, two basic additive technologies SLS and MJF were generated. The main goal of the thesis was to compare the most promising additive technologies based on plastics in terms of production principle, material, quality, and precision.

By analyzing the experiments carried out to compare the suitability of the AM application and its directions for plastic components, it can be stated that during visual observation, the SLS technology appeared to be a technology that should clearly achieve the best parameters in the quality of the production process, but the following evaluations point to various pitfalls that need to be taken into account when choosing a technology as a production process.

Subsequent experimental results and findings continued through the monitoring of hardness results as one of the key mechanical properties, where various methods were applied to identify character. By far the best comprehensive parameters are shown by MJF samples.

Although the surface texture was suitable for SLS technology as a parameter Ra, MJF technology showed significantly better shape values than Pa, Ra, and Wa. The results were also confirmed by comprehensive data from the working accuracy monitored on samples, where the best values of production process stability were with MJF technology.

A great benefit of the study, in addition to the character of the samples produced and their functional properties, is the design of the 3D models of the samples. The proposal offers a comprehensive view of the monitoring of character traits in the production process and the impact on quality itself. The given sample design is a significant shift in comprehensive evaluation for the selection and application of AM. The samples generate a lot of data that exceeds the capabilities of comprehensive processing within a single study. We assume that the methodology will also be suitable for the identification of knowledge of a research nature, which will contribute to the expansion of theoretical knowledge in AM.

Reference

1. C. A. Chatham, T. E. Long, C. B. Williams, Prog. Polym. Sci. 2019, 93, 68.
2. BS EN ISO/ASTM 52900:2021, Aditívna výroba – Všeobecné princípy – Základy a slovná zásoba, British Standards Institution 2021, s. 38.
3. Campbell, O. Diegel, J. Kowen, N. Mostow, T. Wohlers, I. Fidan, in Wohlers Report 2022 (eds: D. Bourell, J. Rensburg van), Wohlers Associates, Washington DC 2022.
4. F. Lupone, E. Padovano, F. Casamento, C. Badini, Materiály 2022, 15, 183.
5. S. Yuan, F. Shen, C. K. Chua, K. Zhou, Prog. Polym. Sci. 2019, 91, 141.
6. R. Goodridge, S. Ziegelmeier, v Laser Additive Manufacturing – Materials, Design, Technologies and Applications (Ed: Milan Brandt), Elsevier Inc. 2017, s. 181, ISBN 9780081004333, ,https://doi.org/ 10.1016/B978-0-08-100433-3.00007-5.
7. Hewlett-Packard Inc., HP Multi Jet Fusion Technology – A Disruptive 3D Printing Technology for a New Era of Manufacturing – Technical White Paper, Palo Alto, CA, USA, 2018.
8. C. Fleischmann, R. Donovan, S. R. Woodruff, Y. Feng, Trojrozmerná (3D) tlač, 2019, WO 2019/099031 A1.
9. B. Scherer, I. L. Kottenstedde, F. M. Matysik, Monatshefte für Chemie 2020, 151, 1203.
10. Z. Xu, Y. Wang, D. Wu, K. P. Ananth, J. Bai, J. Manuf. Proces. 2019, 47, 419.
11. EOS GmbH Electro Optical Systems, FORMIGA P 110 Velocis, Krailling, DE 2022.
12. M. Mele, G. Campana, G. L. Monti, Modelling of the capillarity effect in Multi Jet Fusion technology, Additive Manufacturing volume 30, ISSN 2214-8604 https://doi.org/10.1016/j.addma.2019.100879, 2019 100879, pp1-9.
13. Hewlett-Packard Inc., HP Jet Fusion 5200 Series 3D Printing Solutions, Palo Alto, CA, USA 2019.
14. H. J. O'Connor, A. N. Dickson, D. P. Dowling, Addit. Manuf. 2018, 22, 381.
15. T. Palma, M. Munther, P. Damasus, S. Salari, A. Beheshti, K. Davami, J. Manuf. Proces. 2019, 40, 76.
16. C. S. Abbott, M. Sperry, N. B. Crane, J. Manuf. Proces. 2021, 70, 55.
17. Y. Chen, A. Chen, J. Wright, A. Fitzhugh, A. Hartman, J. Zeng, G. X. Gu, Adv. Eng. Mater. 2022, 24, 2270033.
18. K. Chen, Z. H. Koh, K. Q. Le, H. W. B. Teo, H. Zheng, J. Zeng, K. Zhou, H. Du, Virtual Phys. Prototyp. 2022, 17, 631.
19. B. Sagbas, B. E. Gümüş, Y. Kahraman, D. P. Dowling, J. Manuf. Proces. 2021, 70, 290.
20. J. Riedelbauch, D. Rietzel, G. Witt, Addit. Manuf. 2019, 27, 259.
21. M. Galati, F. Calignano, S. Defanti, L. Denti, J. Manuf. Proces. 2020, 57, 244.
22. M. Mele, G. Campana, G. L. Monti, Addit. Manuf. 2019, 30, 100879.
23. M. Mele, G. Campana, G. Pisaneschi, G. L. Monti, Rýchly prototyp. J. 2020, 26, 1789.
24. H. W. B. Teo, K. Chen, V. T. Tran, H. Du, J. Zeng, K. Zhou, Polymér 2021, 235, 124256.
25. S. Rosso, R. Meneghello, L. Biasetto, L. Grigolato, G. Concheri, G. Savio, Addit. Manuf. 2020, 36, 101713.
26. C. Cai, W. S. Tey, J. Chen, W. Zhu, X. Liu, T. Liu, L. Zhao, K. Zhou, J. Mater. Proces. Technol. 2021, 288, 116882.
27. F. Calignano, F. Giuffrida, M. Galati, J. Manuf. Proces. 2021, 65, 271.
28. G. Craft, J. Nussbaum, N. Crane, J. P. Harmon, Addit. Manuf. 2018, 22, 800.
29. H. J. O' Connor, D. P. Dowling, Addit. Manuf. 2020, 31, 100961.
30. B. Guo, Z. Xu, X. Luo, J. Bai, Virtual Phys. Prototyp. 2021, 16, S39.
31. Sharebot S.r.l., https://www.sharebot.it/stampanti/snowwhite-2/ #technical-details (prístup: marec 2023).
32. Hewlett-Packard Inc., Príručka HP MJF – Všeobecné odporúčania pre tlačové procesy, Palo Alto, Kalifornia, USA 2019.

33. M. Mele, G. Campana, G. L. Monti, Rýchly prototyp. J. 2021, 27, 1138.
34. R. D. Goodridge, C. J. Tuck, R. J. M. Hague, Prog. Mater. Sci. 2012, 57, 229.
35. Baesso, D. Karl, A. Spitzer, A. Gurlo, J. Günster, A. Zocca, Addit. Manuf. 2021, 47, 102250.